Predicting Phase Synchronization of Non-phase-coherent Chaos

Isao T. Tokuda[1], Jürgen Kurths[2,3], István Z. Kiss[4] and John L. Hudson[5]

[1] *School of Information Science, Japan Advanced Institute of Science and Technology, Ishikawa 923-1292, Japan.*
[2] *Department of Physics, Humboldt University Berlin, Newtonstr. 15, 12489 Berlin, Germany.*
[3] *Potsdam Institute for Climate Impact Research, Telegraphenberg A 31, 14473 Potsdam, Germany.*
[4] *Department of Chemistry, Saint Louis University, 3501 Laclede Ave., St. Louis, MO 63103-2010, USA.*
[5] *Department of Chemical Engineering, University of Virginia, 102 Engineers' Way, Charlottesville, VA 22904, USA*

PACS 05.45.Tp – Time series analysis
PACS 05.45.Xt – Synchronization; coupled oscillators
PACS 82.40.Bj – Oscillations, chaos, and bifurcations

Abstract. - A new approach is presented for the reconstruction of phase synchronization phenomena from measurement data of two coupled chaotic oscillators. The oscillators are assumed to be non-phase coherent, making the synchronization analysis extremely difficult. To deal with such non-phase-coherent systems, a CPR index has been recently developed based on the idea of recurrence plot. The present study combines a nonlinear modeling technique with the CPR index to recover the synchronization diagram of non-phase-coherent oscillators. Lyapunov exponents are also utilized to locate the onset point of synchronization. This allows the prediction of the regime of phase synchronization as well as non-synchronization in a broad parameter space of coupling strength without further experiments. The efficiency of this technique is demonstrated with simulated data from two coupled Rössler oscillators as well as with experimental data from electrochemical oscillators.

Introduction. – Synchronization is a fundamental phenomenon of coupled nonlinear oscillators, which are common in nature and engineering. Based on the type of the element, the studies of synchronization can be classified mainly into coupled limit cycle oscillators and coupled chaotic oscillators. For limit cycle oscillators, there exists a standard methodology to analyze the coupled system. The famous example is the phase reduction theory of weakly coupled limit cycles [1]. Theoretical and experimental investigations have been also made on the coupled chaotic oscillators. Up to date, four basic types of synchronization have been found, namely, complete synchronization [4, 5], generalized synchronization [6, 7], phase synchronization [8], and lag synchronization [9]. Phase synchronization (PS) has found many applications including laboratory experiments as well as natural systems [2, 3]. For wider applications to real-world problems, the next important step is to analyze the PS phenomena from time series data observed from experimental or natural systems. So far, several techniques have been developed to detect PS in the underlying coupled nonlinear systems from bivariate or multivariate data [2, 10–12]. Although such techniques have been shown to be quite efficient even for noisy and non-stationary data, the problem of modeling the synchronization phenomena from data remains open. By using such models, it is of special interest to infer a synchronization diagram, which yields the regimes of PS, non-PS, and borderlines between them, which are dependent upon the system parameters such as the coupling strength and the parameter mismatch. By recovering such a synchronization diagram from a few sets of experimental data, a deeper insight into the underlying coupled systems can be gained. This problem formulation is quite practical in situations, under which an extensive synchronization experimentation is not possible or very expensive and only limited data sets can be recorded. Parkinson tremor [11] and Epileptic seizure [13] are the good examples, since conditions or the strong synchrony induced within neuronal elements should be predicted *a priori* to prevent the diseases. Another interesting example is the structural engineering problem, well known as the crowd synchrony of the London Millennium Bridge [14]. On the opening day of the bridge, unexpected swaying motion has been induced by the collective motion of the massive crowds walking on the bridge. Prior detection of such coherent motion is desired for the stable bridge design.

To retrieve the synchronization regime, the construction of a nonlinear model, which is parameterized by a forcing condition such as the coupling strength, from the recorded data is required. In a recent study, we have introduced a basic approach for constructing such a parameterized family of models based on nonlinear prediction technique [15]. This approach has the important practical advantage that no prior knowledge of the parameterized family of the underlying dynamics is necessary. Our technique has been successfully applied to prototypical PS models and to experimental data from a paced plasma discharge tube [15] and from a chaotic CO_2 laser [16]. It is important, however, to note that these studies have dealt only with phase-coherent chaotic systems, whose phase can be easily computed due to the existence of a unique rotation center of the dynamics. This cannot be always expected for real-world systems, which typically give rise to more complicated dynamics often associated with non-phase-coherent property. Hence the aim of the present Letter is to develop a novel technique to recover the synchronization diagrams of non-phase-coherent systems.

Although it is in general not straightforward to extract phase for non-phase-coherent systems, there exist some methods to detect PS without directly computing the phases. One approach is to utilize the Lyapunov exponents, one of which turns from zero to negative value at the onset of PS [2, 17]. As another index for detecting the PS, we focus on a synchronization index (CPR), which has been newly developed based on recurrence probabilities of recurrence plot [18]. The use of the CPR index is promising, since the computational procedure is relatively simple and it has been shown to be applicable quite well to non-phase-coherent systems even with noisy and instationary data. By combining the nonlinear modeling technique with the CPR index, we show that the synchronization diagrams of the coupled non-phase-coherent chaos can be well reconstructed.

Problem and Method. – Consider two diffusively coupled nonlinear oscillators

$$\dot{\mathbf{x}}_{1,2} \quad = \quad \mathbf{f}_{1,2}(\mathbf{x}_{1,2}) + \mathbf{c}\ (\mathbf{x}_{2,1} - \mathbf{x}_{1,2}), \qquad (1)$$

where $\mathbf{f}_{1,2}$ and $\mathbf{x}_{1,2}$ represent dynamics and state vector of the first or second oscillator, respectively. The coupling matrix $\mathbf{c}$ is composed of $c_{i,j} = C\ (i = j = 1)$; 0 (otherwise), whose strength is controlled by the constant parameter C. Without the coupling ($C = 0$), each oscillator $\mathbf{f}_{1,2}$ is assumed to give rise to non-phase-coherent chaotic dynamics. Suppose that from the two oscillators, bivariate time series $\{\xi_1(t), \xi_2(t)\}$ are obtained using the first component of the state vector, *i.e.* $\xi_i = \mathbf{I}\mathbf{x}_i$ ($\mathbf{I} = [1, 0, \cdots, 0]$). For simplicity, we restrict our problem to the situation that the dynamical variable involved in the coupling $\mathbf{C}(\mathbf{x}_{2,1} - \mathbf{x}_{1,2})$ is observed as the time series, since this fits to many practical experiments. More general case of observing an arbitrary dynamical variable has been studied in [15], to which our framework can be extended. The sampling interval is denoted as Δt. Depending upon the coupling strength, the coupled oscillators can generate a PS as well as a non-PS regime. The bivariate time series are measured under a few conditions associated with different coupling strengths C_i ($i = 1, \cdots, M$). Our task is to infer a synchronization diagram, which classifies the parameter space of the coupling strength into regimes of PS and non-PS, only from such a few measurement data. Our primary assumptions are: (i) the underlying dynamical equations (1) are unknown but the system is known to be diffusively coupled, (ii) the dynamical variables involved in the diffusive coupling are measured as the time series, and (iii) the coupling constants C_i associated with the measurements are known and they are taken from a non-synchronous regime.

Now we describe our modeling technique. First, we embed the bivariate time series $\{\xi_1(t), \xi_2(t)\}$ into delay coordinates $\mathbf{X}_1(t) = \{\xi_1(t), \xi_1(t-\tau), \ldots, \xi_1(t-(d-1)\tau)\}$, $\mathbf{X}_2(t) = \{\xi_2(t), \xi_2(t-\tau), \ldots, \xi_2(t-(d-1)\tau)\}$ (d: embedding dimension, τ: time lag) and suppose according to the embedding theorem [19] that the original coupled oscillators of Eq. (1) are transformed into the following dynamics

$$\dot{\mathbf{X}}_{1,2}(t) = \mathbf{F}_{1,2}(\mathbf{X}_{1,2}(t), C\ (\mathbf{X}_{2,1}(t) - \mathbf{X}_{1,2}(t))). \qquad (2)$$

Note that this transformation cannot be assumed if the condition (ii) does not hold. The main point of our modeling is to construct a set of nonlinear functions $\tilde{\mathbf{F}}_{1,2}$, that approximate Eq. (2). If the original dynamics (1) is well embedded in the delay coordinate space and the embedded dynamics is precisely modeled, the synchronization structure of the original dynamics can be predicted by analyzing the model $\tilde{\mathbf{F}}_{1,2}$.

For the construction of the nonlinear models, there exist various functional systems that approximate the nonlinear dynamics, such as polynomial functions [20], radial basis functions [21], artificial neural networks [23], and local linear models [22]. The local models are not suitable for the modeling of global dynamics such as bifurcations due to their inherent local property. Global functional models are preferred here. As one of the most typical global models, this study exploits the neural network. It should be noted here that the other global models can be also utilized for the present study and our purpose is not to develop an application specific to neural networks. Our modeling procedure consists of the following main steps.

(P1) The embedding dimension d and the time lag τ are chosen. To determine the time lag, the first zero-crossing point of the autocorrelation function, which is commonly used for the nonlinear data analysis [24], is exploited. The embedding dimension can be determined by conventional dimensional analysis [24].

(P2) Each nonlinear function $\tilde{\mathbf{F}}_i : R^d \times R^d \to R^d$ ($i = 1, 2$) is realized by a 3-layer feed-forward neural network [23], having $2d$-units in the input layer, d-units in the output layer, and h-units in the middle layer. Each neural network has $4dh$ parameters, denoted as ω, which are optimized to fit into the data as follows. First, the cost

function is defined as

$$E(\omega) = \sum_{i=1}^{M}\sum_{j=1}^{d}\sum_{t}\sum_{s=1}^{S}|\mathbf{X}_j(t+s\Delta t, C_i) - \tilde{\mathbf{X}}_j(t+s\Delta t, C_i)|^2, \quad (3)$$

where $\tilde{\mathbf{X}}_j$ is the trajectory in the interval $[t, t+S\Delta t]$, generated from the model equations

$$\dot{\tilde{\mathbf{X}}}_{1,2}(t) = \tilde{\mathbf{F}}_{1,2}(\tilde{\mathbf{X}}_{1,2}(t), C\,(\tilde{\mathbf{X}}_{2,1}(t) - \tilde{\mathbf{X}}_{1,2}(t))) \quad (4)$$

started from the initial condition $\tilde{\mathbf{X}}_{1,2}(t) = \mathbf{X}_{1,2}(t)$. The maximal integration time is set as $S = 5$. To minimized the cost function, the quasi-Newton method based upon the Broyden-Fletcher-Goldfarb-Shanno formula with Luenberger's self-scaling [25] is utilized. To computed first derivatives of the cost function, variational equations of the model equations (4) are numerically integrated.

(P3) By repeating the procedure (P2), Q sets of different nonlinear models $\tilde{\mathbf{F}}_{1,2}^{(i)}$ $(i = 1, \cdots, Q)$ are obtained, which have the same neural network architecture but different parameter values ω optimized with random initial conditions. Then, the ensemble average is taken as

$$\bar{\mathbf{F}}_{1,2} = \frac{1}{Q}\sum_{i=1}^{Q}\tilde{\mathbf{F}}_{1,2}^{(i)}. \quad (5)$$

It has been shown that the ensemble technique provides much more reliable modeling of nonlinear dynamics compared to the case of utilizing only a single model, whose results are rather sensitive to the optimized parameters [26].

(P4) CPR index is computed [18]. By free-running the model equations $\dot{\tilde{\mathbf{X}}}_{1,2}(t) = \bar{\mathbf{F}}_{1,2}(\tilde{\mathbf{X}}_{1,2}(t), C\,(\tilde{\mathbf{X}}_{2,1}(t) - \tilde{\mathbf{X}}_{1,2}(t)))$, a pair of trajectories $\{\tilde{\mathbf{X}}_{1,2}(t)\}_{t=1}^{N}$ can be generated. Then, the generalized autocorrelation function is obtained for each trajectory as $P_i(\tau) = \sum_{t=1}^{N-\tau}\Theta(\epsilon - |\tilde{\mathbf{X}}_i(t) - \tilde{\mathbf{X}}_i(t+\tau)|)/(N-\tau)$, where ϵ is a threshold and Θ is the Heaviside function. The threshold ϵ is determined in such a way that the recurrence rate is kept constant, *i.e.*, $\sum_{t=1}^{N}\sum_{s=1}^{N}\Theta(\epsilon - |\tilde{\mathbf{X}}(t) - \tilde{\mathbf{X}}(s)|)/N^2 = 15$ %. The CPR index can be computed as the cross correlation between $P_1(\tau)$ and $P_2(\tau)$ as $CPR =< \bar{P}_1(\tau)\bar{P}_2(\tau) > /(\sigma_1\sigma_2)$, where $\bar{P}_{1,2}$ means that the mean value is subtracted and $\sigma_{1,2}$ are the standard deviations of $P_{1,2}(\tau)$. If the system is in synchronization, the generalized autocorrelation functions of the two trajectories get strongly correlated, resulting in a high $CPR{\approx}1$. Otherwise a low CPR is expected.

By changing the coupling strength C, we may finally draw the synchronization diagram, showing the dependence of the CPR index on the coupling strength C.

Applications. – First, we applied our method to simulated data from two coupled Rössler oscillators [17]: $\dot{x}_{1,2} = -\alpha_{1,2}y_{1,2} - z_{1,2}$, $\dot{y}_{1,2} = \alpha_{1,2}x_{1,2} + ay_{1,2} + C(y_{2,1} - y_{1,2})$, $\dot{z}_{1,2} = 0.1 + z_{1,2}(x_{1,2} - 8.5)$. The parameter mismatch was set as $\alpha_{1,2} = 1{\pm}0.02$. In the case of $a = 0.16$, each Rössler oscillator gives rise to phase-coherent chaotic dynamics. Under two conditions with different coupling strength $C = 0$ and $C = 0.025$, which are in a non-PS regime, the bivariate data $\{y_1(t), y_2(t)\}$ were measured. As reported in [15, 27], data from a PS regime should not be used for the modeling, since they provide only a limited dynamical information constrained in the synchronization manifold. For each condition, 800 data points were collected with the sampling interval of $\Delta t = 0.2$. To examine the effect of observational noise, *Gaussian* noise was added to the bivariate data. The noise level was varied as 5, 10, 15, and 20 %. Following the modeling procedure (P1), the embedding dimension and the time lag were set as $(d, \tau) = (3, 0.8)$ Note that the embedding dimension was not a crucial modeling parameter, since essentially the same results have been obtained with $d = 4$. For the construction of the neural networks in procedure (P2), number of the units in the middle layer was set as $h = 8$.

Fig. 1 (a) shows the synchronization diagram reconstructed by the ensemble model $\bar{\mathbf{F}}_{1,2}$, averaged over 5 nonlinear models. No noise was added to the data sets. Overall structure of the reconstructed diagram is in a very good agreement with the one drawn by simulating the original coupled Rössler equations (solid line with circles). As indicated by the arrow at $C{\approx}0.037$, the sudden drop of the CPR-index corresponds to the onset point of PS. The nonlinear model locates almost the same onset point as the original system. This demonstrates the strong capability of recovering the synchronization diagram in the case of modeling the noise-free data.

Figs. 1 (b) and (c) show the Lyapunov exponents (λ_1, λ_2, λ_3, λ_4) computed for the original system (sold lines) and the nonlinear model (dotted lines) by using the standard numerical technique [28]. A clear onset point of PS is discernible also in these figures. Namely, the first and second exponents (λ_1, λ_2) remain to be positive in this range of coupling (except for the periodic window observed in the nonlinear model at $C{\approx}0.067$), implying that both of the coupled oscillators are chaotic in the amplitude. Whereas the third Lyapunov exponent (λ_3) stays on the zero line, the fourth Lyapunov exponent (λ_4) turns from zero to negative at $C{\approx}0.037$, which is a clear transition to PS. The Lyapunov spectrum analysis is therefore consistent with the CPR index, which also locates the onset point of PS at $C{\approx}0.037$.

Fig. 1 (d) shows the case of applying the nonlinear modeling in the presence of 5, 10, 15, and 20 % noise. Up to the noise level of 15 %, the model predicts the onset point roughly at around the correct one. Only under the very strong level of 20 % noise, the model becomes rather inaccurate, resulting in the prediction of the onset point smaller than the correct one. This implies that the present approach is quite robust against a moderate amount of observational noise, which is important for the real data analysis.

Next, we examined the case of $a = 0.2925$ that generates a funnel-type chaotic attractor. Due to the non-phase-coherent property, it is nontrivial to detect PS in

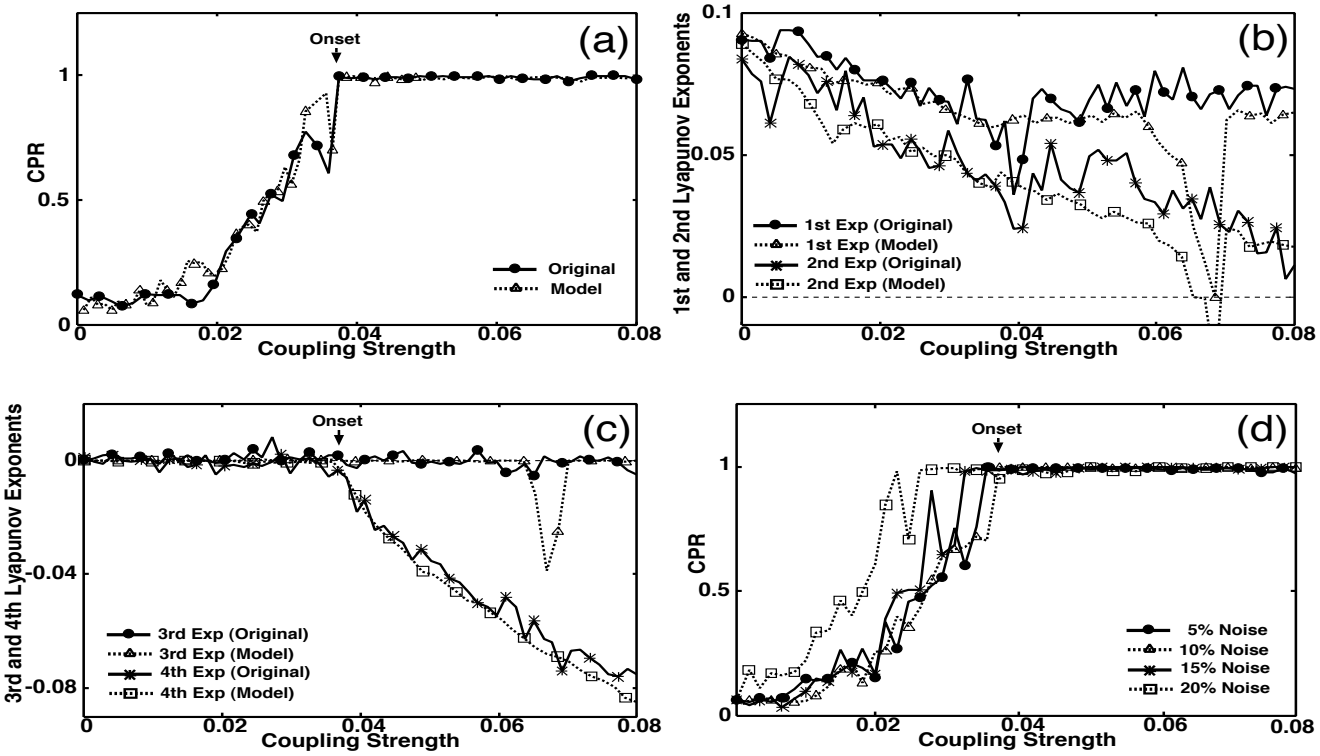

Fig. 1: Phase-coherent Rössler chaos. (a): CPR index drawn by varying the coupling strength in the range of $C \in [0, 0.08]$ for the original two coupled Rössler oscillators (sold line with filled circles) and for the nonlinear model obtained from noise-free data (dotted line with triangles). (b), (c): First, second, third, and fourth Lyapunov exponents computed for the original Rössler oscillators (sold lines) and the nonlinear model obtained from noise-free data (dotted lines). (d): The CPR curves for nonlinear models obtained from noisy data (5 % noise: solid line with circles; 10 % noise: dotted line with triangles; 15 % noise: solid line with asterisks; 15 % noise: dotted line with squartes). The arrows of (a), (c), and (d) indicate the onset point of PS at $C = 0.037$.

this case. Advantage of utilizing the CPR index is that it can be applied also to the non-phase-coherent systems. In the same manner as the phase-coherent case, the bivariate data were collected under the coupling strength of $C = 0$ and $C = 0.02$, both of which are in a non-PS regime. Fig. 2 (a) shows the synchronization diagram reconstructed by the ensemble model $\bar{\mathbf{F}}_{1,2}$, averaged over 5 nonlinear models, under a noise-free condition (dotted line) and the one drawn from the original equations (solid line). Due to the non-phase-coherency, the original diagram exhibits a relatively noisy curve. However, a clear onset of PS is recognized at $C \approx 0.18$. The diagram reconstructed by the nonlinear model reproduced the qualitative structure of the original diagram very precisely with a correct prediction of the PS onset point. In Fig. 2 (b), the second and third Lyapunov exponents (λ_2, λ_3) are computed for the original system (sold lines) and the nonlinear model (dotted lines). As studied in detail in [17], the coupled Rössler oscillators in this funnel regime gives rise to generalized synchronization and PS almost simultaneously. Namely, at $C \approx 0.18$, the third Lyapunov exponent turns from zero to negative, indicating the onset of PS. Almost at the same place, the second Lyapunov exponent turns from positive to zero, which indicates the onset of generalized synchronization. Almost the same transition can be observed also in the nonlinear model. This implies the strong modeling capability of predicting both generalized synchronization and PS by the present approach.

Figs. 2 (b) and (c) show the results of the nonlinear modeling in the presence of 5, 10, 15, and 20 % noise. As the noise level is increased, we see that the model prediction based on the CPR index gets inaccurate, locating the onset point of PS at smaller couping values. This can be confirmed also in Figs. 2 (e) and (f), where the turning points of the second and third Lyapunov exponents, which indicate the onset of generalized synchronization and PS, are found at relatively smaller values. This implies that the inaccurate prediction of the PS is not due to the CPR measure but to the modeling error. Despite this modeling difficulty, the prediction error of the onset point was less than 16 % for the noise level of 5 and 10 %. Taking into account the moderate amount of 10 % noise as well as the difficulty of detecting PS in non-phase-coherent systems, we consider that the present approach is robust enough to be applied to the real-world systems.

Let us finally apply our technique to experimental data.

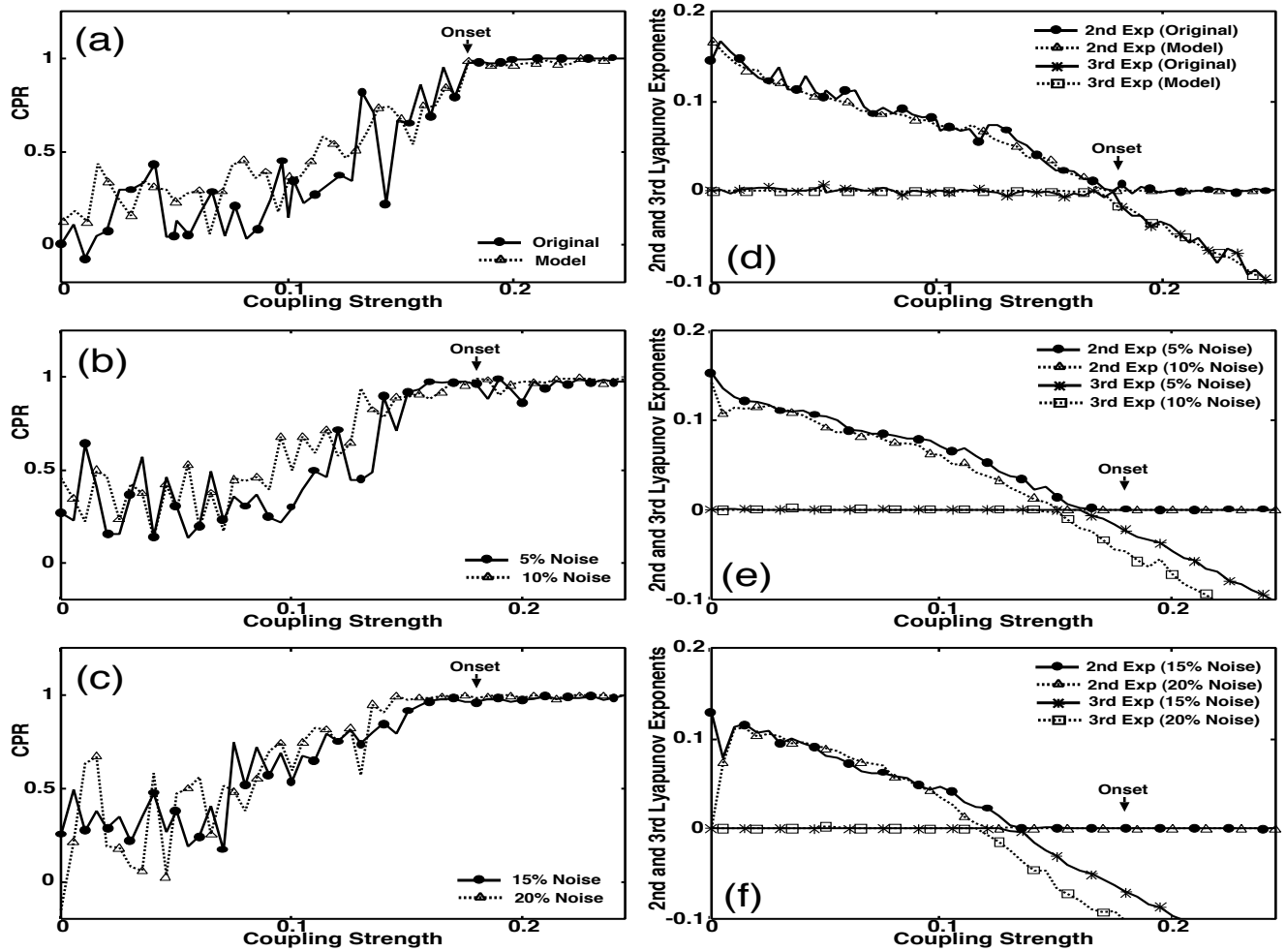

Fig. 2: Non-phase-coherent Rössler chaos. (a), (b), (c): CPR index drawn by varying the coupling strength in the range of $C \in [0, 0.25]$ for the original two coupled Rössler oscillators (sold line of (a)) and for the nonlinear models obtained from noise-free data (dotted line of (a)), data with 5 % and 10 % noise (solid and dotted lines of (b)), and data with 15 % and 20 % noise (solid and dotted lines of (c)). (d), (e), (f): Second and third Lyapunov exponents computed for the original Rössler oscillators (sold lines of (d)) and for the nonlinear models obtained from noise-free data (dotted lines of (d)), data with 5 % and 10 % noise (solid and dotted lines of (e)), and data with 15 % and 20 % noise (solid and dotted lines of (f)). The arrows indicate the onset point of PS at $C \approx 0.18$.

We use an electrochemical oscillator system, in which the interaction between two non-phase-coherent chaotic oscillators has been well designed [29]. The experiments were carried out in a standard three-compartment electrochemical cell consisting of two iron working electrodes (1-mm diameter each with 2-mm spacing), a $Hg/Hg_2SO_4/K_2SO_4$ reference, and a Pt counter electrode. The applied potential (V) of both electrodes were connected to the potentiat through two individual parallel resistors (R_{ind}) and through one series collective resistor (R_{coll}) which furnishes a global coupling of strength $K = R_{ind} \ / \ R_{tot}$, where $R_{tot} = R_{coll} + R_{ind} \ / \ 2$ is kept constant. For $K = 0$, the external resistance furnishes no additional coupling; for $K = 1$, the maximal external coupling is achieved. This global coupling can be translated into the diffusive coupling as $C = K/(1 + K)$.

From the current of each electrode, three sets of bivariate time series $\{\xi_1(t), \xi_2(t)\}$ were measured (sampling frequency: 2 kHz; data points: 2400) under the coupling strength of $K = 0, 0.2, 0.4$, which are all in a non-synchronized regime. Following the modeling procedure, the embedding dimension and the time lag were set as $(d, \tau) = (4, 35[\text{ms}])$. For construction of the neural network, the number of the units in the middle layer was set as $h = 12$. The ensemble model was then constructed from $Q = 50$ nonlinear models. Fig. 3 compares the synchronization diagram of the nonlinear model (dotted line) with that of the experimental data (solid line). The model provides a highly precise prediction on the onset point of the PS at $C = 0.6$, which agrees with the preceding studies [18, 29]. Although the nonlinear model becomes unstable (divergent solution) at $C = 0.65$, the qualitative

structure of the original synchronization diagram is well reproduce until that point. This demonstrates the strong potential of the present method to real experimental data.

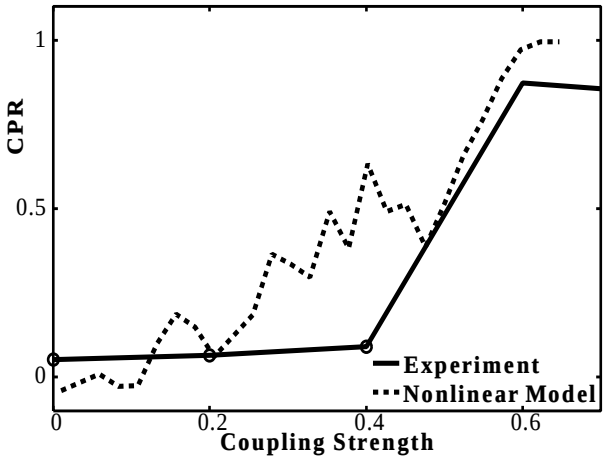

Fig. 3: Synchronization diagram of the two coupled electrochemical oscillators (solid line) and the model prediction (dotted line). The location of the data used for the modeling is indicated by the three circles.

Summary. – To summarize, a new approach has been presented for the reconstruction of PS from measurement data of coupled non-phase-coherent chaotic oscillators. For simulated data from two coupled Rössler oscillators in a funnel-type chaotic regime, the synchronization diagram has been recovered only from few data sets. The method was robust up to 10 % observational noise. The results with experimental data from electrochemical oscillators demonstrated its practical applicability to real-world data. Our future study will focus on the application of this methodology to biological data.

* * *

The authors would like to thank Prof. Parlitz, Dr. Romano, and Dr. Thiel for helpful discussions. This work was supported in part by the National Science Foundation under grant CBET-0730597 and by the Ministry of Internal Affairs and Communications (MIC) of Japan under grant SCOPE-071705001. I.T. was supported by the Alexander-von-Humboldt Foundation for the research fellowship. J.K. was supported by EU BioSim Network of Excellence.

REFERENCES

[1] Y. Kuramoto, *Chemical Oscillations, Waves and Turbulence* (Springer, Berlin, 1984).
[2] A. Pikovsky, M. Rosenblum, and J. Kurths, *Synchronization - A Universal Concept in Nonlinear Sciences*, (Cambridge University Press, Cambridge, 2001).
[3] J. Kurths (Ed.), *Phase Synchronization and its Applications*, Special Issue in Int. J. Bifurcation and Chaos, **10-11** (2000).
[4] H. Fujisaka and T. Yamada, Prog. Theor. Phys. **69** (1983) 32.
[5] L.M. Pecora and T.L. Carroll, Phys. Rev. Lett. **64** (1990) 812.
[6] N.F. Rulkov, M.M. Sushchik, L.S. Tsimring, and H.D.I. Abarbanel, Phys. Rev. E **51** (1995) 980.
[7] L. Kocarev and U. Parlitz, Phys. Rev. Lett. **76** (1996) 1816.
[8] M.G. Rosenblum, A.S. Pikovsky, and J. Kurths, Phys. Rev. Lett. **76** (1996) 1804.
[9] M.G. Rosenblum, A.S. Pikovsky, and J. Kurths, Phys. Rev. Lett. **78** (1997) 4193.
[10] C. Schafer, M.G. Rosenblum, J. Kurths, and H.-H. Abel, Nature **392** (1998) 239.
[11] P. Tass, M. G. Rosenblum, J. Weule, J. Kurths, A. S. Pikovsky, J. Volkmann, A. Schnitzler, and H. J. Freund: Phys. Rev. Lett. **81** (1998) 3291.
[12] N. Marwan, M. Romano, M. Thiel, and J. Kurths, Phys. Rep. **438** (2007) 237.
[13] K. Lehnertz and C. E. Elger, Phys. Rev. Lett. **80** (1998) 5019.
[14] S. H. Strogatz, D. M. Abrams, A. McRobie, B. Eckhardt, and E. Ott, Nature **438** (2005) 43.
[15] I. Tokuda, J. Kurths, and E. Rosa Jr., Phys. Rev. Lett. **88** (2002) 014101.
[16] I. Tokuda, J. Kurths, E. Allaria, R. Meucci, S. Boccaletti, and F. T. Arecchi, Phys. Rev. E **70** (2004) 035204R.
[17] G. Osipov, B. Hu, C. Zhou, M. Ivanchenko, and J. Kurths, Phys. Rev. Lett. **91** (2003) 024101.
[18] M. C. Romano, M. Thiel, J. Kurths, I. Z. Kiss, and J. L. Hudson, Europhys. Lett. **71** (2005) 466.
[19] F. Takens, in *Dynamical Systems and Turbulence*, Lecture Notes in Math., edited by D. A. Range and L.S. Young (Springer, Berlin, 1981), Vol. 898, p. 366.
[20] J. P. Crutchfield and B. S. McNamara, Complex Systems **1** (1987) 417.
[21] M. Casdagli, Physica **35D** (1989) 335.
[22] J. D. Farmer and J. J. Sidorowich, Phys. Rev. Lett. **59** (1987) 845.
[23] D. E. Rumelhart, J. L. McClelland, and the PDP Research Group, *Parallel Distributed Processing*, (MIT Press, Cambridge, 1986).
[24] H. Kantz and T. Schreiber, *Nonlinear Time Series Analysis*, (Cambridge University Press, Cambridge, 1997).
[25] D. G. Luenberger, *Linear and Nonlinear Programming* (Addison-Wesley, 1973).
[26] I. Tokuda, U. Parlitz, J. Kurths, Int. J. Bifurcation and Chaos **17** (2007) 3557.
[27] I. T. Tokuda, S. Jain, I. Z. Kiss, J. L. Hudson, Phys. Rev. Lett. **99** (2007) 064101.
[28] I. Shimada and T. Nagashima, Prog. Theor. Phys. **61**, 1605 (1979).
[29] I. Z. Kiss, Q. Lv, and J.L. Hudson, Phys. Rev. E **71** (2005) 035201.